Dynamic Optical Power Measurements and Modeling of Light-Emitting Diodes Based on a Photodetector System and Photo-Electro-Thermal Theory

Huanting Chen, Albert T. L. Lee, *Member, IEEE*, Siew-Chong Tan, *Senior Member, IEEE*, and S. Y. Hui, *Fellow, IEEE*

***Abstract*—Optical measurements based on integrating sphere are primary suitable for steady-state measurements and unsuitable for dynamic real-time measurements. This paper presents an alternative method using the combination of a photodetector system and the dynamic photo-electro-thermal theory for real-time optical measurements. It is demonstrated that the voltage output of a photodetector can be correlated to the optical power in real time. Such method has been successfully applied to analyze a phosphor-converted white light-emitting diode (PC white LED) using an extended dynamic model with separate calculations of optical power from the blue LED chips and phosphor layer. Both calculated and practical results are included to confirm the validity of the new method.**

***Index Terms*—Passive LED systems, photo-detector systems, photo-electro-thermal theory for LED systems.**

I. Introduction

WITH rapid advancements of light emitting diode (LED) devices, drivers and system theory, LED technology has replaced the traditional light sources such as incandescent and discharge lamps in many sectors of the lighting market. In lighting industry, it is a common practice to house the light source or lighting system inside an integrating sphere for optical measurements. Such optical power measurement method has been recommended by the International Commission on Illumination (CIE) in the technical report CIE 127:2007, which standardizes the measurement procedures of measuring optical

Manuscript received February 28, 2018; revised May 15, 2018, July 16, 2018, September 14, 2018, and November 13, 2018; accepted December 27, 2018. Date of publication January 3, 2019; date of current version June 28, 2019. This work was supported in part by the Hong Kong Research Grant Council under the Theme-based research project: T22-715-12N and in part by the Natural Science Foundation for Distinguished Young Scholars of Fujian Province under Grants 2016J06016 and IRTSTFJ. Recommended for publication by Associate Editor B. Lehman. *(Corresponding author: S. Y. Hui.)*

H. Chen is with the College of Physics and Information Engineering, Minnan Normal University, and Fujian Optoelectronic Materials and Devices Application Technology Development Base, Zhangzhou 363000, China (e-mail:

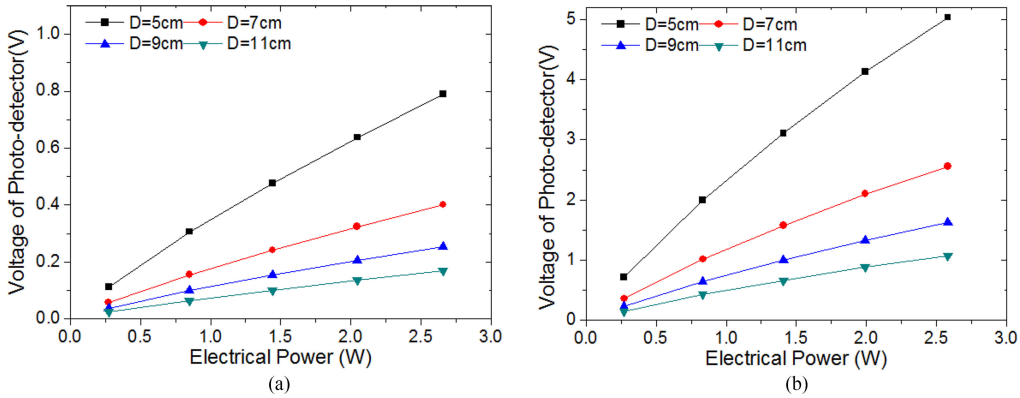

Fig. 1. Response voltage of photodetector versus electrical power of LED with different distance. (a) Blue LED. (b) PC white LED.

an LED system at steady and dynamic conditions. The proposed model is extended with the use of optical transfer in the phosphor and blue LED chip layer to determine the optical power of blue LED and phosphor independently. A faster measurement procedure consisting of a simple optical and electrical power measurement based on the use of the photodetector and oscilloscope. Based on this procedure, the optical power of the phosphor and blue LED and the heat dissipation coefficient of white LED can be estimated independently. The parameters obtained in this fast procedure are verified by integrating sphere measurement. The proposed model is then used for performance analysis and comparative study on the dynamic optical and color variation of the passive LED system with current ripple effect.

II. Optical Power Flow Between LED Source and Photodetector System

The optical power received ($P_{\mathrm{opt,r}}$) by the photodetector is dependent on the solid-angle (Ω) subtended by the photodetector. The LED source is assumed as a point source. The light intensity leaving a point source decreases in proportion to the inverse of the distance from the source, as shown in (1). The solid-angle (Ω) is approximately the area of the photodetector (A) divided by the distance (D) squared from the LED source to photodetector

$$\Omega = \iint \sin\theta \mathrm{d}\theta \mathrm{d}\varphi = 2\pi\left(1-\cos\theta\right) \cong \frac{\mathrm{A}}{\mathrm{D}^2}. \tag{1}$$

The received optical power ($P_{\mathrm{opt,r}}$) of photodetector can be expressed as

$$P_{\mathrm{opt,r}} = \varepsilon P_{\mathrm{opt,t}}\Omega \tag{2}$$

where ε is the relational coefficient between emitting optical power within the solid angle Ω and the received optical power. Each type of LED has unique angular dependence of output power distribution. The different angular properties of LED sources are dependent on the coefficient of ε. The $P_{\mathrm{opt,t}}$ is the total optical power of LED source and can be measured by integrating sphere. Tested at four different distances between the LED source and the photodetector, the voltage responses of photodetector are measured when the LED source is powered at different electrical power levels. All measurements are made under steady state. The parameters are measureable from existing commercial lighting instruments. By fitting the parameters (measured from steady-state conditions) into the framework of the proposed model, we can predict the optical power from the blue LED chips and phosphor layer. The measured results are shown in Fig. 1. It can be seen that the photodetector voltage decreases with the distance between the LED source and the photodetector. It is caused by the incident angle from the LED source to the photodetector. The total optical power of the LED source versus photodetector voltage is plotted in Fig. 2.

The received optical power $P_{\mathrm{opt,r}}$ is directly proportional to the photodetector voltage V_{p}, which can be shown as follows:

$$V_p = \alpha P_{\mathrm{opt,r}} = \alpha\varepsilon P_{\mathrm{opt,t}}\Omega = \alpha\varepsilon P_{\mathrm{opt,t}}\frac{A}{D^2} \tag{3}$$

where α is the relational coefficient between the received optical power and the photodetector voltage. It is noted that α is different with wavelength distribution. The relationships between $P_{\mathrm{opt,t}}/V_{\mathrm{p}}$ and the distance in (3) are established in Fig. 3. With a given distance between LED source and photodetector, the total optical power can be obtained under the measured dynamic voltage of photodetector.

Equation (3) can be rewritten as

$$P_{\mathrm{opt,t}} = \frac{D^2}{A\alpha\varepsilon}V_p = \beta_c V_p \tag{4}$$

where β_{c} is conversion coefficient that is dependent on the distance between photodetector and LED source.

Based on the results of Fig. 3, the optical power of phosphor and blue LED of PC white LED can be individual measured and calculated by using the response voltage of photodetector. It is a new measured method for determining the optical power by employing the characteristics of photo-electro system, which is different from the traditional method of integrating sphere. In this experiment, two high-power LED samples of the same package and same batch are used for the investigation. Each LED sample composes of a blue LED chip and a yellow phosphor coating (under a transparent silicone cover). The first sample has the transparent silicone cover without the phosphor coating so that it is used as a blue LED for comparison. It is termed as "blue LED" in this paper. The second LED sample has the phosphor-converted and is termed as "PC white LED."

The light output of blue LED is not the same as blue light leaving LED die into the phosphor inside the white LED since the latter case is subject to back-scattering and associated extra losses. In order to simplify the proposed model with negligible multiple reflection and scattering, the optical power of blue LED

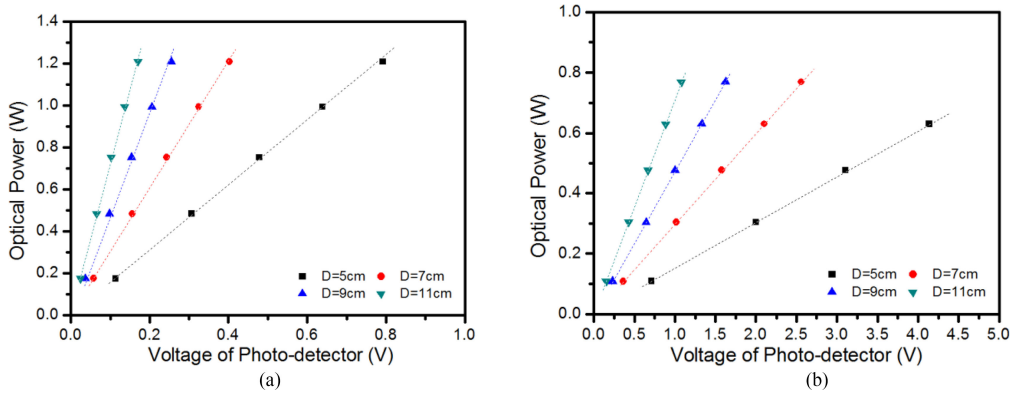

Fig. 2. Response voltage of photodetector versus total optical power of LED with different distance using by integrating sphere measurement. (a) Blue LED. (b) PC white LED.

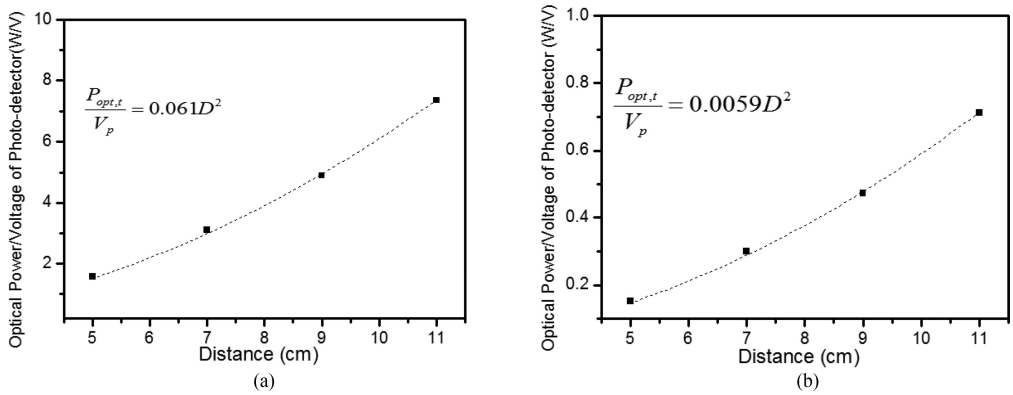

Fig. 3. Distance between LED source and photodetector versus optical power/photodetector voltage. (a) Blue LED. (b) PC white LED.

can be assumed to be same as the optical power leaving LED die into the phosphor inside white LED.

The energy of the converted yellow light dissipates during its propagation in the phosphor layer follows the Lambert–Beer's law [12]. It is pointed out that the Lambert–Beer's law is only applicable to the weak scattering system [13]. In the weakly scattering regime with $\mathrm{L}/\,l_{tr} \ll 1$ (the sample thickness L and the transport mean free path l_{tr}), the transport of light is analytically described by the venerable Lambert–Beer law. In scattering systems, such as white LEDs with $\mathrm{L}/\,l_{tr} \approx 1$, light is scattered multiple times and diffused. In previous works [14], [15], the enhanced backscattering system, a quintessential multiple scattering phenomenon, was calculated both with exact theory and with diffusion theory. Even for weak multiple scattering, the diffusion theory agrees to better than 10% with the exact results. The theoretical method is effective but not precise enough, since the multiple reflection is not seriously considered in Lambert–Beer law. This causes the optical constants to be larger than the actual values. It should be pointed out that the proposed model did not include multiple reflection and scattering. It assumes a weakly scattered system, which can be explained by using the Lambert–Beer's law.

The emitting optical power of the blue LED is $P_{\mathrm{opt,t(b)}}$, according to the boundary conditions, the emitting optical power of blue light propagation across the phosphor layer $P_{\mathrm{opt,b(w)}}$ can be rewritten as

$$P_{\mathrm{opt,b(w)}} = P_{\mathrm{opt,t(b)}} \times e^{-\alpha_B h} \tag{5}$$

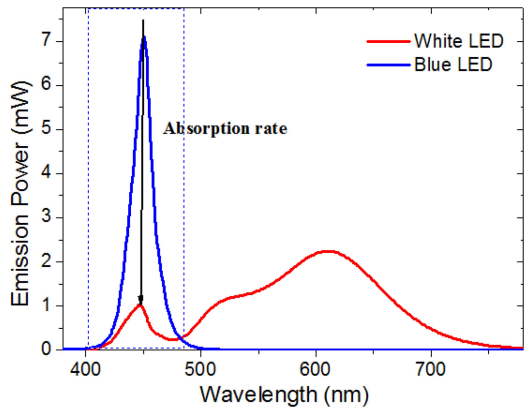

Fig. 4. Spectrum power distribution of white LED and blue LED.

where α_{B} is a coefficient of blue light absorption in the phosphor layer and h is the thickness of phosphor layer. $P_{\mathrm{opt,b(w)}}$ represents the blue light power emitting out of the PC white LED package. If the $\exp(-\alpha_{\mathrm{B}} h)$ can be assumed as the absorption rate γ_{B},. (5) can be rewritten as

$$\frac{P_{\mathrm{opt,b(w)}}}{P_{\mathrm{opt,t(b)}}} = \gamma_B . \tag{6}$$

The absorption rate γ_{B} can be extracted from the measured spectrum of blue LED and PC white LED, as shown in Fig. 4. A series of optical and thermal measurements are carried out to investigate the relationship between absorption rate γ_{B} and current/heatsink temperature. It should be noted that α_{B} and

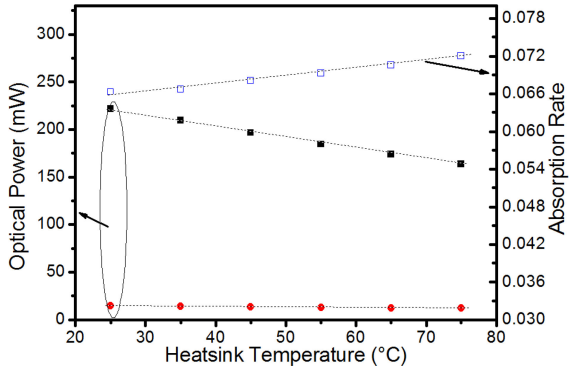

Fig. 5. Optical power and absorption rate for blue LED with different heatsink temperatures under constant current.

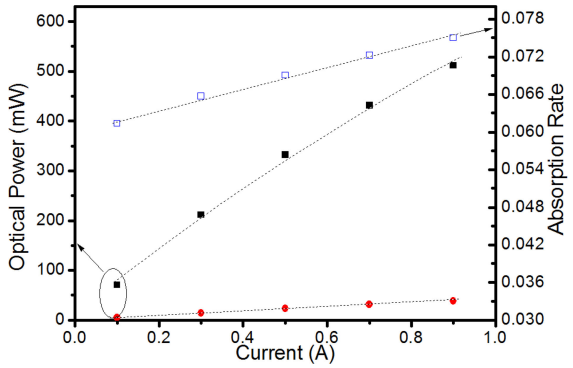

Fig. 6. Optical power and absorption rate for blue LED with different currents under constant heatsink temperature.

γ_{B} are specific model parameters and not characteristics of the phosphor material.

The temperature-controlled heatsink enables the temperature of the mounting plate (on which the LED device is placed) to be controlled. In the practical operating range, the relationship of the absorption rate γ_{B} as a function of the heatsink temperature T_{hs} for constant LED current I_0 operation is fairly linear and can, therefore, be approximated as a linear relationship

$$r_B(T_{\mathrm{hs}}, I_0) = a_1 T_{\mathrm{hs}} + a_2 \tag{7}$$

where a_1 is a constant representing the slope and a_2 is another constant. Both a_1 and a_2 can be obtained from the measurements in Fig. 5.

To establish the dependence of the absorption rate γ_{B} on the LED current, the LED device is operated at constant heatsink temperature. Using the integrating sphere optical system, the practical measurements of the absorption rate γ_{B} as a function of the LED current are obtained and shown in Fig. 6. It can be seen that the absorption rate γ_{B} increases as the injection current rises. In practice, the absorption rate γ_{B} is approximately linearly proportional to the injection current at constant heatsink temperature $T_{\mathrm{hs},0}$. So the absorption rate γ_{B} can be obtained as a linear function of I

$$r_B(T_{\mathrm{hs},0}, I) = b_1 I + b_2 \tag{8}$$

where b_1 and b_2 are constants that can be extracted from Fig. 5 with constant heatsink temperature.

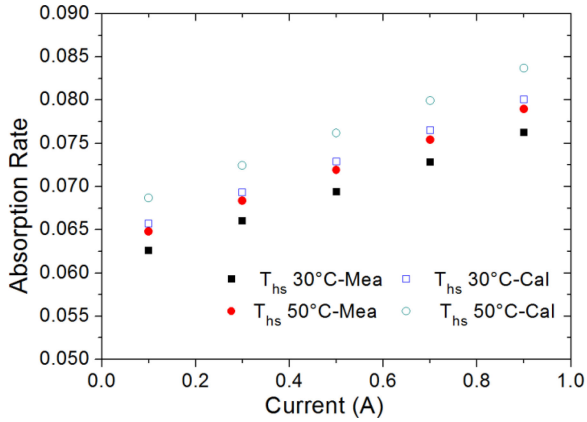

Fig. 7. Measured and calculated absorption rate for blue LED with different current and heatsink temperature.

Therefore, the function of absorption rate γ_{B} can be constructed as in the following equation:

$$r_B(T_{\mathrm{hs}}, I) = \frac{(b_1 I + b_2)(a_1 T_{\mathrm{hs}} + a_2)}{c} \tag{9}$$

where c is intersection value of function for (7) and (8). This intersection value is the value of absorption rate γ_{B} at point ($T_{\mathrm{hs},0}$,I_0). It should be noted that (9) can be used to estimate the absorption rate γ_{B} of the blue LED at a given range of heatsink temperature (from 25 to 75 °C) and injection current (from 0.1 to 0.9 A). Equation (9) links the absorption rate γ_{B} to the injection current and heatsink temperature together.

Based on (9), the calculated absorption rate curves are plotted along with the measurements in Fig. 7. The average deviation between the calculation and the measurement is about 5.6%. The maximum deviation between the calculation and the measurement is 8.3%. The calculated values using the proposed model are generally more consistent with the measurements. It is pointed out that absorption rate in Figs. 5–7 is also LED specific and only valid in the context of the modeling of a particular LED device.

According to (9), optical power of the phosphor layer for the PC white LED can be expressed as

$$\begin{aligned} P_{\mathrm{opt,p(w)}} &= P_{\mathrm{opt,t(w)}} - P_{\mathrm{opt,b(w)}} = P_{\mathrm{opt,t(w)}} - \gamma_B P_{\mathrm{opt,t(b)}} \\ &= P_{\mathrm{opt,t(w)}} - \frac{(b_1 I + b_2)(a_1 T_{\mathrm{hs}} + a_2) P_{\mathrm{opt,t(b)}}}{c} \\ &= \frac{D^2}{A\alpha\varepsilon} V_{\mathrm{p,w}} - \frac{(b_1 I + b_2)(a_1 T_{\mathrm{hs}} + a_2) \frac{D^2}{A\alpha\varepsilon} V_{\mathrm{p,b}}}{c} \\ &= \beta_{\mathrm{c,w}} V_{\mathrm{p,w}} - \frac{(b_1 I + b_2)(a_1 T_{\mathrm{hs}} + a_2) \beta_{\mathrm{c,b}} V_{\mathrm{p,b}}}{c} \end{aligned} \tag{10}$$

where $P_{\mathrm{opt,t(w)}}$ and $P_{\mathrm{opt,t(b)}}$ represent the optical power of the PC white LED and blue LED, respectively. $P_{\mathrm{opt,b(w)}}$ represents the blue light power emitting out of the PC white LED package. where $\beta_{\mathrm{c,w}}$ and $\beta_{\mathrm{c,b}}$ represent conversion coefficient of PC white LED and blue LED, respectively, $V_{\mathrm{p,w}}$ and $V_{\mathrm{p,b}}$ represent photodetector voltage of PC white LED and blue LED, respectively.

Under steady-state conditions [3], the steady-state heatsink temperature $T_{\rm hs}$ can be expressed as

$$T_{\rm hs} = T_a + {\rm NP}_d k_h R_{\rm th}^{\rm hs-a} \tag{11}$$

where $T_{\rm a}$ is ambient temperature, $R_{\rm th}^{\rm hs-a}$ is the thermal resistance of the heatsink, P_d is the heat dissipation of the LED, $k_{\rm h}$ is the heat dissipation coefficient, N is the number of LEDs.

Putting (11) into (10), optical power of the phosphor layer for the PC white LED can be rewritten as

$$\begin{aligned} P_{\rm opt,p(w)} &= P_{\rm opt,t(w)} - P_{\rm opt,b(w)} = P_{\rm opt,t(w)} - \gamma_B P_{\rm opt,t(b)} \\ &= P_{\rm opt,t(w)} - \frac{(b_1 I + b_2)\left(a_1 T_{\rm hs} + a_2\right) P_{\rm opt,t(b)}}{c} \\ &= \frac{D^2}{A\alpha\varepsilon} V_{\rm p,w} - \frac{(b_1 I + b_2)\left(a_1 T_{\rm hs} + a_2\right) \frac{D^2}{A\alpha\varepsilon} V_{\rm p,b}}{c} \\ &= \beta_{\rm c,w} V_{\rm p,w} \\ &\quad - \frac{(b_1 I + b_2)\left[a_1\left(T_a + N R_{\rm th}^{\rm hs-a} P_d k_h\right) + a_2\right] \beta_{\rm c,b} V_{\rm p,b}}{c}. \end{aligned} \tag{12}$$

Several important observations should be noted from (12) as follows:

1) Equations (12) relates the emitting optical power of the phosphor layer for the PC white LED $P_{\rm opt,p(w)}$ to the injection current of LED I, the thermal resistance of heatsink $R_{\rm th}^{\rm hs-a}$, the conversion coefficient of PC white LED and blue LED ($\beta_{\rm c,w}$ and $\beta_{\rm c,b}$), the photodetector voltage of PC white LED and blue LED ($V_{\rm p,w}$ and $V_{\rm p,b}$), and electrical-thermal parameters of the system (a_1, a_2, b_1, b_2, and c) altogether.
2) For a given injection electrical power $P_{\rm d}$, the emitting optical power of phosphor layer for PC white LED $P_{\rm opt,p(w)}$ is dependent on the conversion coefficient of PC white LED and blue LED ($\beta_{\rm c,w}$ and $\beta_{\rm c,b}$) and heat dissipation coefficient $k_{\rm h}$.
3) However, no quantitative modeling has been previously reported to relate the response voltage of photodetector to the emitting optical power of phosphor layer for PC white LED. Therefore, (12) provide a new mathematical relationship linking the electrical power and thermal effect of LED source with the photo-electro conversion of photodetector. This important equation enables researchers and engineers to use a photodetector system, instead of an integration sphere, to determine optical power measurement.

III. Practical Estimation of Optical Power of Phosphor Layer Based on Photodetector System (Without Using Integrating Sphere)

In order to check the validity of (12), a photo-sensor circuit has been set up as shown in Fig. 8. The output voltage of the photodetector circuit is monitored and recorded by a digital storage oscilloscope. A high-power PC-based white LED device and a blue LED are mounted on their respective heatsinks of known thermal resistance values. The LED device is driven by the output of an operational amplifier, which in principle can inject ac and/or dc current into the LED device. The optical signal emitted by the LED is received by a silicon photodetector

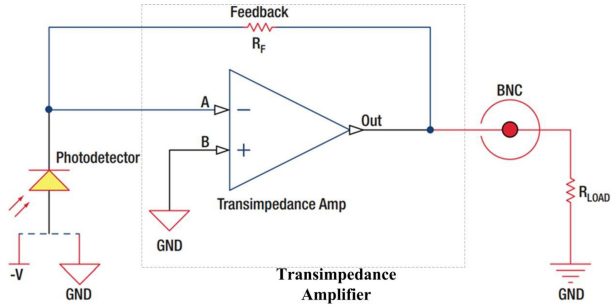

Fig. 8. Circuit diagram of the photodetector circuit [16].

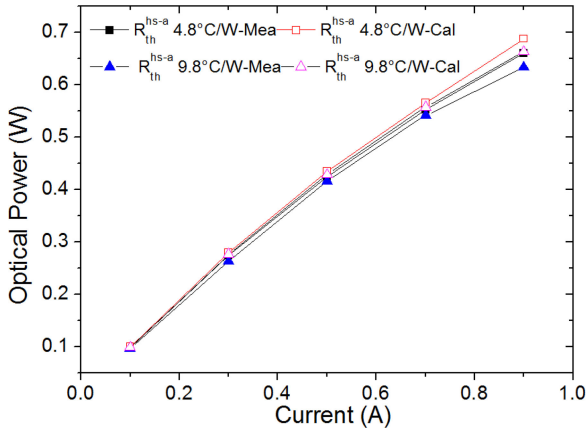

Fig. 9. Measured and calculated optical power of the phosphor layer for PC white LED mounted on a heatsink ($R_{\rm th}^{\rm hs-a}$ 4.8 °C/W and $R_{\rm th}^{\rm hs-a}$ 9.8 °C/W) as a function of LED current.

with 10 MHz bandwidth [16]. The real-time voltage waveforms of photodetector circuit can be captured by the oscilloscope under different LED current levels.

While output voltage measured from the photodetector system provides data for (12) to generate the calculated optical power value, traditional optical power measurements based on the use of the integrating sphere are also obtained in order to compare with the calculated values based on the photodetector system. Therefore, the LED samples with different injection currents are mounted on a Peltier-cooled fixture that is attached to an integrating sphere in accordance with the recommendations of CIE [17]. The Peltier-cooled fixture is used to stabilize the LED temperature for the optical measurements and it also served as an actively temperature-controlled cold-plate for thermal measurements. Optical measurements of LED samples are performed in thermal and electrical steady-state conditions with the HASS-2000 spectroradiometer system. The light output is measured after driving LED with current for 20 min with heatsink temperature being kept at constant.

The parameters of the photodetector system are tabulated in Table I. Putting these parameters into (12), the theoretical optical power of the phosphor layer for PC white LED $P_{\rm opt,p(w)}$ as a function of LED power can be derived. Based on calculated values using (12) and practical measurements using the integrating sphere, two sets of calculated and measured optical power of the phosphor layer for PC white LED $P_{\rm opt,p(w)}$ as a function of LED power are shown in Fig. 9, when the LED device is mounted on two heatsinks with different thermal resistance

TABLE I
REQUIRED PARAMETERS FOR THE PHOTODETECTOR SYSTEM

$\beta_{c,w}$	$\beta_{c,b}$	a_1	a_2	b_1	b_2	c	k_h	$R_{th}^{hs\text{-}a}$ (°C/W)	N	T_a(°C)
$0.0059D^2$	$0.061D^2$	0.000118	0.0629	0.01688	0.0602	0.0657	0.59-0.71	6.8	1	25

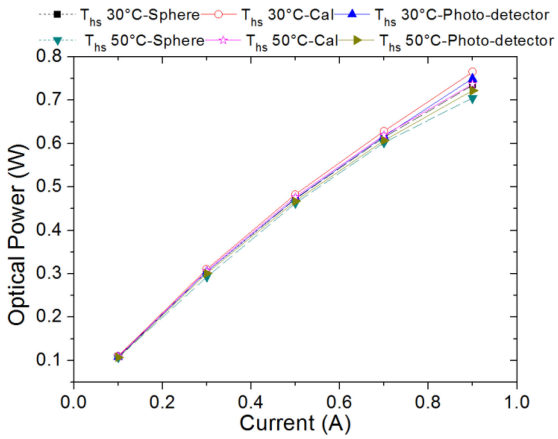

Fig. 10. Measured and calculated optical power of PC white LED with different heatsink temperature using by integrating sphere and photodetector.

values. It can be seen that the variation of the optical power of phosphor layer for PC white LED $P_{\mathrm{opt,p(w)}}$ is highly dependent on the change of junction temperature and electrical power, and this affects the performance of the phosphor layer. The average deviation between the calculations and measurements is about 3.7%. The maximum deviation between the proposed model and the measurement is 7.6%. The calculated values using the proposed model are generally consistent with the measurements.

For the heatsink thermal resistance of 4.8 °C/W, optical power of the phosphor layer $P_{\mathrm{opt,p(w)}}$ is about 0.099 W at an LED current of 0.1 A. When the injection current is 0.9 A, $P_{\mathrm{opt,p(w)}}$ increases to 0.66 W. For the heatsink thermal resistance of 9.8 °C/W and an LED current of 0.9 A, $P_{\mathrm{opt,p(w)}}$ only decreases to 0.63 W, which means the variation $P_{\mathrm{opt,p(w)}}$ with injection current of 0.9 A is about 4.7% for LED source with heatsink thermal resistance of 4.8 and 9.8 °C/W. This practical result highlights the important fact that optical power of the phosphor layer decreases with increasing heatsink resistance. It is noted that the variation of the optical power of the phosphor layer with electrical power and heatsink thermal resistance are kept within obvious ranges. If the thermal design is not restricted by space, a big heatsink with low $R_{\mathrm{th}}^{\mathrm{hs-a}}$ should always be selected for the LED system in order to effectivly reduce the overall optical power of phosphor layer variation. In Fig. 10, measured and calculated optical power of PC white LED with different heatsink temperature used by integrating sphere and photodetector are shown. The calculated values using the proposed model and measured results based on photodetector system are generally consistent with the integrating sphere measurements.

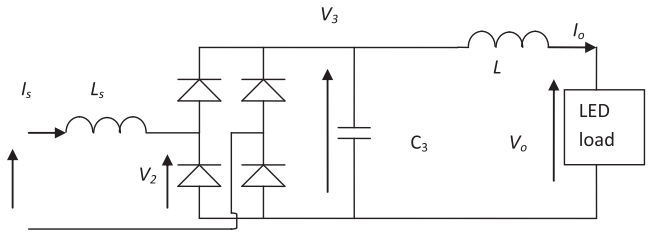

Fig. 11. Example of passive offline LED driver for general lighting [18].

IV. ESTIMATION OF OPTICAL AND COLOR VARIATION OF A PASSIVE LED SYSTEM WITH DYNAMIC CURRENT RIPPLE BASED ON PHOTODETECTOR SYSTEM

Sections II and III describe the estimation of the "steady-state" optical power emitted from the phosphor layer of the white LED system based on the steady condition using by proposed model. While (1)–(12) mathematically link up the steady-state relationship of photometric, electrical, and thermal aspects of the LED system with the photo-electro conversion of photodetector based on the steady state model, they do not include the effect of time, which is a critical factor, particularly in view of the behavior of the optical power and CCT decline with time in previous LED system installations. Users of LED systems could also be misled by the high initial optical power they see without realizing that the optical power level may drop significantly as the heatsink temperature increases gradually. Based on the dynamic model that includes the thermal capacitance of the LED package and the heatsink, the dynamic PET theory has been developed to incorporate the effect of time.

In practice, there may be variation of optimal power and other radiometric and colorimetric variables in modern LED systems. For example, Chen *et al.* [18] show that the PET theory can be used to design passive LED system (see Fig. 11), which has no closed-loop control, to generate light output with minimized luminous flux variation even though there are double-frequency ripples in the LED current and power.

It is imperative to use the dynamic model for checking radiometric and thermal performance in an LED system design. The idea is to ensure that the LED system will provide sufficient optical power and CCT to meet the required specifications and that the instantaneous junction temperature of the LED device will not exceed the maximum temperature rating stipulated in the manufacturers' data sheets.

The dynamic output power (as a function of time) of the passive LED system can be used as the input of the dynamic model. This time-domain output power and light output function of the passive LED system can be obtained from practical measurements and calculations based on inputs from the

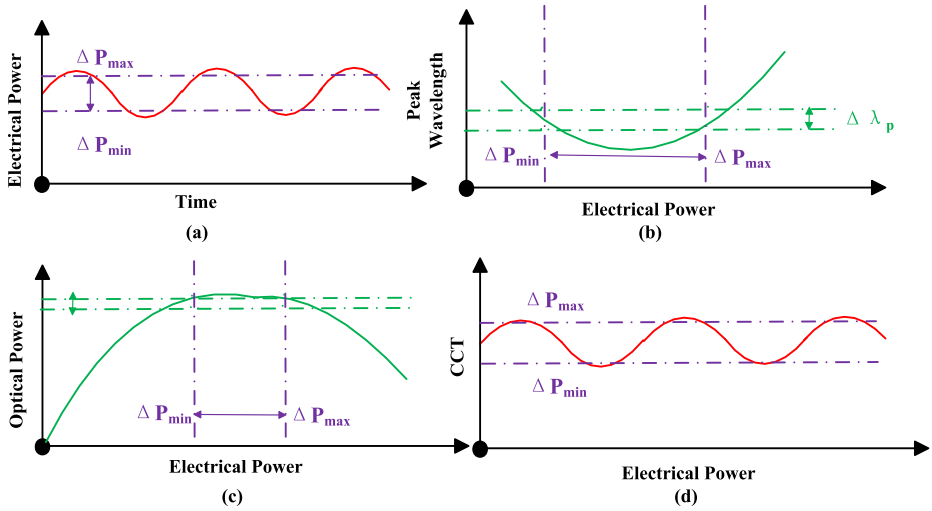

Fig. 12. (a) Power fluctuation of passive LED system with time. (b) Typical characteristics of peak wavelength variation with electrical power. (c) Example of reducing optical power variation using the top region of the light-power curve. (d) Example of reducing CCT variation using the bottom region of the peak wavelength-power curve.

photodetector system. The junction temperature and CCT with current ripple can then be predicted as a function of time. The optical power and peak wavelength function has a similar parabolic nature with input power according to PET theory [3], [19], as shown in Fig. 12. Beyond the maximum light output operating point, further increase in the LED power will lead to light drop. This characterisitc function of the steady-state PET theory has been practically verified in [3] and [19]. The slope of the parabolic curve at and around the peak value is relatively small. If the LED power is controlled within the specified range as indicated in Fig. 12(b) and (c), the variation of the peak wavlength and light output is minimal. This is an important and unique feature of LED system that differentiates LED from other general lighting systems.

The parabolic curve of the optical power and peak wavelength versus LED power in Fig. 12 opens a new opportunity to design passive LED system with minimum optical power and CCT fluctuation. The slope of the parabolic curve at and around the peak value is relatively small. If the LED power is controlled within the specified range, the variation of the optical power and CCT is minimal. This is an important and unique feature of passive LED system that is different from active LED system used in road lighting systems.

The experimental setup is to verify dynamic current ripple of the passive LED system. The passive LED system is placed 50 cm away from the photodetector. The optical signal emitted by the passive LED system was received by a silicon photodetector. This photodetector converts light into a voltage signal instantaneously so that the dynamic variation of the light output can be captured by a digital oscilloscope. The instantaneous power and current waveforms of the passive LED system driven at 50 Hz with input ac voltage of 220 V and measured response voltage of photodetector are captured in Fig. 13.

For the passive LED system, the input power is pulsating at twice the mains frequency. Although design engineers can use the heatsink temperature to predict the average internal junction temperature of the LED devices, such average temperature, even if it is lower than the recommended maximum values, cannot guarantee reliable operation of the LEDs. The proposed dynamic PET modeling technique will highlight some common mistakes made in the design stage and serve as a passive LED system design tool for lighting industry. It can cope with the reduction of luminous flux from initial to steady-state operations and predict the internal junction temperature of the LED system will be very useful to passive LED system designers.

The dynamic model includes the thermal capacitance of the LED package and the heatsink, the dynamic PET theory has been developed to incorporate the effect of time. The dynamic junction temperature and luminous flux have been shown in [20] as follows, Eqn. (13) shown at the bottom of this page:

The $T_{\rm j}$ described by formula (13) is the average junction temperature. LED systems with multiple LED devices essentially comprise multiple heat sources at different locations. Even though mounted on the same heatsink, each LED has a different junction temperature, which is dependent on its optical property, operating current, and physical location. A three-dimensional PET-LED nodal model is proposed for the LED system with non-uniform thermal distribution of the heatsink [21]. This LED nodal model can be used to represent the LED array structure on the same heatsink and predict the photometric, electric, and thermal behaviors of the LED system. The calculated non-uniform junction temperature distribution of LED system can

$$T_j = \left\{ \begin{array}{l} -R_{\rm jc} k_h P_d \left(\dfrac{C_{\rm jc} \mathrm{NR}_{\rm th}^{\rm hs-a}}{C_{\rm jc} R_{\rm jc} - C_{\rm hs} R_{\rm th}^{\rm hs-a}} + 1 \right) e^{-\frac{t}{C_{\rm jc} R_{\rm jc}}} - k_h P_d \left(\dfrac{-\mathrm{NR}_{\rm th}^{\rm hs-a} R_{\rm jc} C_{\rm jc}}{C_{\rm jc} R_{\rm jc} - C_{\rm hs} R_{\rm th}^{\rm hs-a}} + \mathrm{NR}_{\rm th}^{\rm hs-a} \right) e^{-\frac{t}{C_{\rm hs} R_{\rm th}^{\rm hs-a}}} \\ + \left(R_{\rm jc} + \mathrm{NR}_{\rm th}^{\rm hs-a} \right) k_h P_d + T_a \end{array} \right\} \quad (13)$$

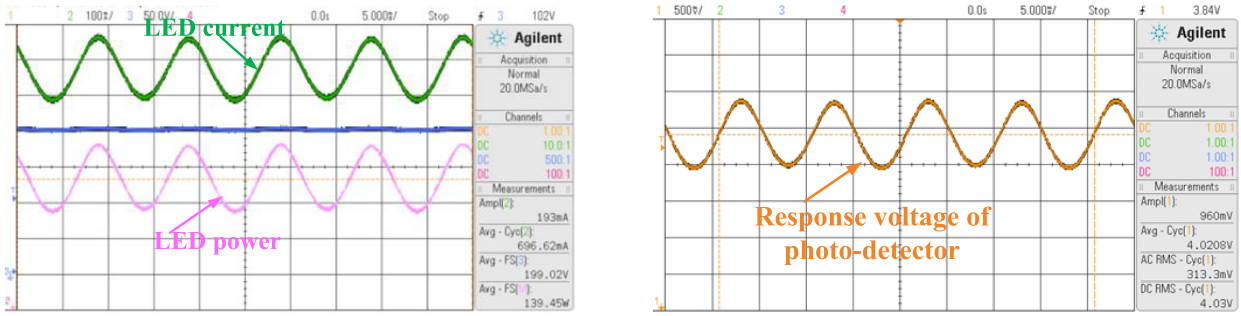

(a) (b)

Fig. 13. (a) Measured LED voltage (blue: 50 V), current (green: 100 mA/div), and power (pink) of the passive LED system driven at 50 Hz and input ac voltage of 220 V. (b) Measured response voltage (yellow: 500 mV/div) of photodetector.

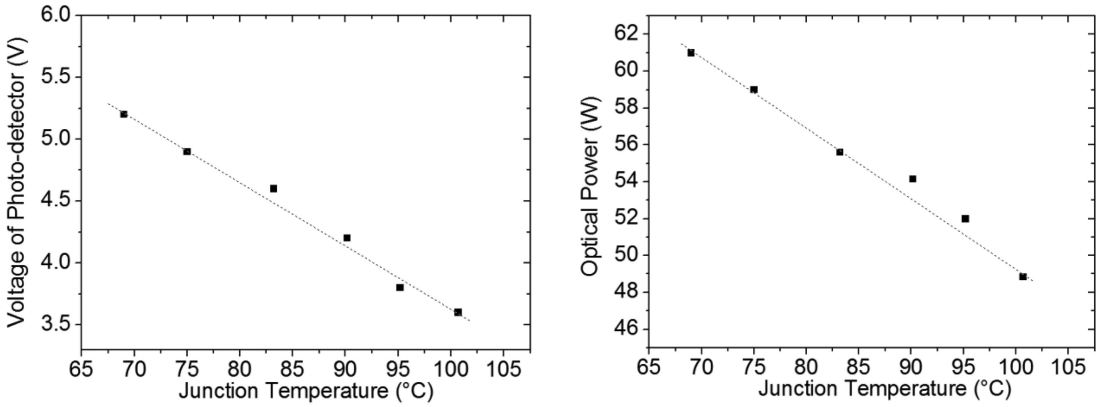

(a) (b)

Fig. 14. (a) Correlation between voltage of photodetector and junction temperature. (b) Correlation between optical power and junction temperature.

be predicted. In very large systems, the calculated non-uniform junction temperature significantly increases the efficiency of the computation, thereby, greatly reduces the required computation time as compared to the calculated average junction temperature, at the expense of reduced accuracy. Therefore, in deciding the approach, a balance should be struck between calculation time and accuracy. Therefore, the calculated average junction temperature is applicable to the LED system for its accuracy and acceptable calculation time.

The mathematical relationship between the voltage of photodetector/optical power and junction temperature for the LED system can be determined as shown in Fig. 14. The linear behavior voltage between photodetector/optical power and junction temperature is clearly shown. The relationship can be expressed as

$$V_p = \alpha_{\mathrm{p,j}} T_j + \beta_{\mathrm{p,j}} \tag{14}$$

$$P_{\mathrm{opt}} = \alpha_{\mathrm{opt,j}} T_j + \beta_{\mathrm{opt,j}} \tag{15}$$

where $\alpha_{\mathrm{p,j}}$ and $\beta_{\mathrm{p,j}}$ are the relational coefficients between the junction temperature and response voltage of photodetector. $\alpha_{\mathrm{opt,j}}$ and $\beta_{\mathrm{opt,j}}$ are the relational coefficients between the junction temperature and optical power. The coefficients can be determined based on the fitting the results of Fig. 14.

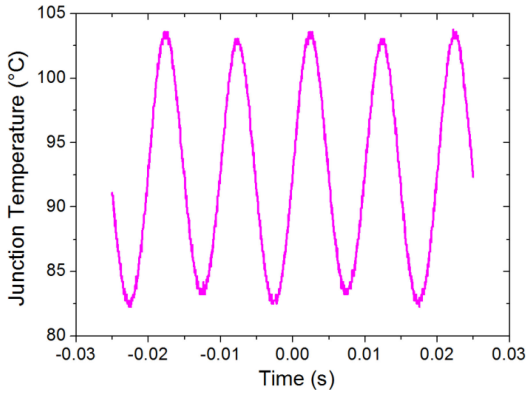

Fig. 15. Calculated junction temperature of the passive LED system.

Putting (14) into (4), the optical power with junction temperature can be expressed as

$$P_{\mathrm{opt}} = \frac{D^2}{A\alpha\varepsilon} V_p = \beta_c V_p = \beta_c \left(\alpha_{\mathrm{p,j}} T_j + \beta_{\mathrm{p,j}}\right). \tag{16}$$

Putting (13) into (16), the optical power with time can be expressed as (17) shown at the bottom of next page.

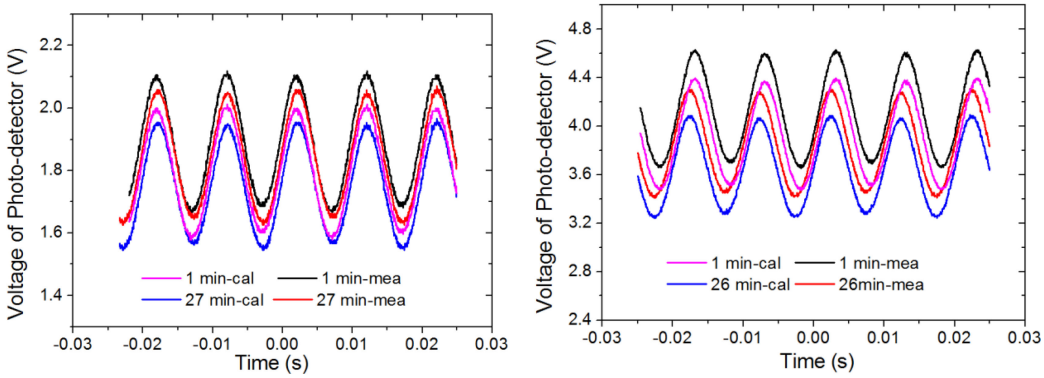

Fig. 16. Calculated and measured response voltage of photodetector at different intervals after turning ON the passive LED system with different input power. (a) Input ac voltage of 140 V. (b) Input ac voltage of 220 V.

The CIE 1931 color system is the root of colorimetry. The tristimulus values X, Y, and Z can be normalized as

$$\begin{cases} x = \dfrac{X}{X+Y+Z} \\ y = \dfrac{Y}{X+Y+Z} \\ z = \dfrac{Z}{X+Y+Z}. \end{cases} \tag{18}$$

Using McCamy's formula, the CCT value can be obtained from the chromaticity coordinates [22]

$$\mathrm{CCT} = 449n^3 + 3525n^2 + 6823.3n + 5520.33 \tag{19}$$

where $n = \frac{(x-0.3320)}{(0.1858-y)}$.

It is noted that the junction temperature of LED system could affect the CCT as reflected by the variation of the chromaticity coordinates. Therefore, putting the dynamic junction temperature of (13) into (19), the CCT with time can be expressed as

$$\begin{aligned} \mathrm{CCT}\left[T_j\left(t\right)\right] &= 449\left(\frac{x\left[T_j\left(t\right)\right]-0.3320}{0.1858-y\left[T_j\left(t\right)\right]}\right)^3 \\ &\quad + 3525\left(\frac{x\left[T_j\left(t\right)\right]-0.3320}{0.1858-y\left[T_j\left(t\right)\right]}\right)^2 \\ &\quad + 6823.3\left(\frac{x\left[T_j\left(t\right)\right]-0.3320}{0.1858-y\left[T_j\left(t\right)\right]}\right) + 5520.33. \end{aligned} \tag{20}$$

All measurements are made under steady state. The parameters are measureable from existing commercial lighting instruments. By fitting the parameters (measured from steady-state conditions) into the framework of the dynamic PET theory, we can predict the transient behavior of optical power and CCT in the time domain.

The output power (as a function of time) of the LED driver can be used as the input of the model. This time-domain output power function of the passive LED system can be obtained from practical measurements. Fig. 11 shows the circuit diagram of the passive LED driver for offline applications. As clearly shown in Fig. 13, the instantaneous power of the passive LED system is not ideal sinusoidal waveforms. The maximum value of each cycle is slightly different. The driving function for the dynamic model shown in (17) and (20) is $P_{\mathrm{d}}(t)$.

Dynamic junction temperature of LED system can be predicted according to dynamic PET theory in (13) and the thermal properties of LED device and heatsink. The corresponding predicted junction temperature variation is plotted in Fig. 15. It can be seen that junction temperature of the passive LED system varies with time. It is important to note that, the average junction temperature is 92.1 °C, but the peak junction temperature is about 103.7 °C, which is still lower than the recommended 125 °C for semiconductor devices. If the peak junction temperature value exceeds the maximum temperature allowed, the thermal design has to be adjusted so as to reduce the peak junction temperature value below its maximum allowable value. Engineers can, therefore, use the dynamic model for the radiometric and thermal check, and fine-tuning the passive LED system design.

Putting the theoretical dynamic junction temperature into junction temperature as a function of voltage of photodetector/optical power, the theoretical dynamic voltage of photodetector/optical power variation as a function of time can be captured. Figs. 16 and 17 show the calculated and measured response voltage of photodetector and optical power, recorded at different intervals after the passive LED system with input ac

$$\begin{aligned} P_{\mathrm{opt}} = \beta_c \alpha_{\mathrm{p,j}} \Bigg\{ & -R_{\mathrm{jc}} k_h P_d \left(\frac{C_{\mathrm{jc}} \mathrm{NR}_{\mathrm{th}}^{\mathrm{hs-a}}}{C_{\mathrm{jc}} R_{\mathrm{jc}} - C_{\mathrm{hs}} R_{\mathrm{th}}^{\mathrm{hs-a}}} + 1 \right) e^{-\frac{t}{C_{\mathrm{jc}} R_{\mathrm{jc}}}} - k_h P_d \left(\frac{-N R_{\mathrm{th}}^{\mathrm{hs-a}} R_{\mathrm{jc}} C_{\mathrm{jc}}}{C_{\mathrm{jc}} R_{\mathrm{jc}} - C_{\mathrm{hs}} R_{\mathrm{th}}^{\mathrm{hs-a}}} + \mathrm{NR}_{\mathrm{th}}^{\mathrm{hs-a}} \right) e^{-\frac{t}{C_{\mathrm{hs}} R_{\mathrm{th}}^{\mathrm{hs-a}}}} \\ & + \left(R_{\mathrm{jc}} + \mathrm{NR}_{\mathrm{th}}^{\mathrm{hs-a}} \right) k_h P_d + T_a \Bigg\} \\ & + \beta_c \beta_{\mathrm{p,j}} \end{aligned} \tag{17}$$

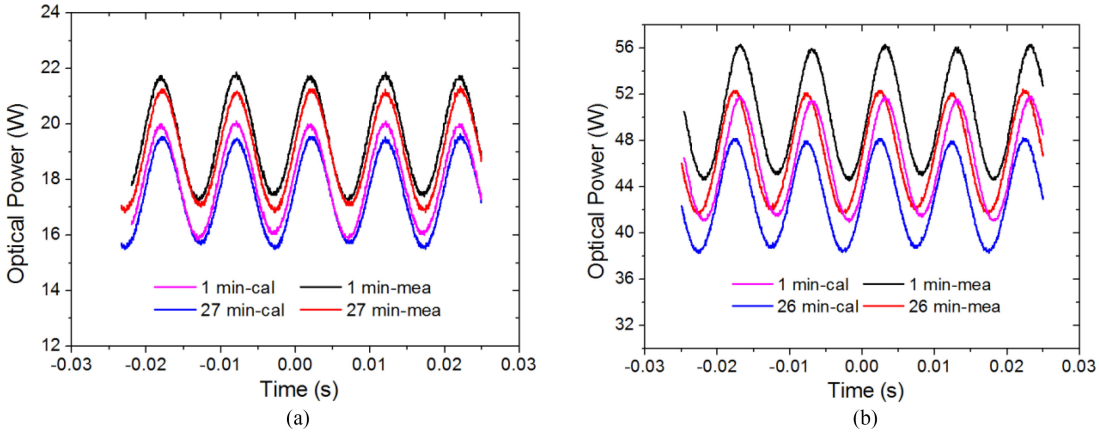

Fig. 17. Calculated and measured optical power of the passive LED system at different intervals with different input power. (a) Input ac voltage of 140 V. (b) Input ac voltage of 220 V.

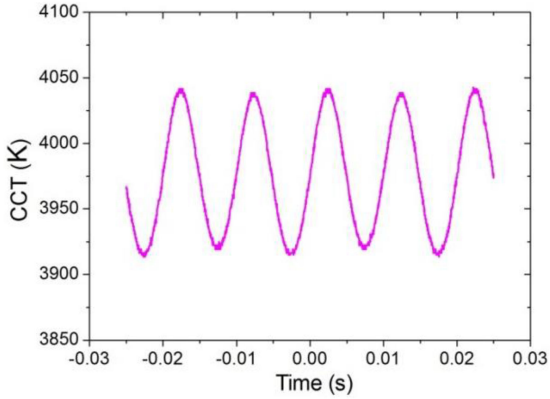

Fig. 18. Predicted CCT of the passive LED system.

voltage of 140 and 220 V has been turned ON. The agreement between measured and calculated results is reasonably good. The maximum relative error between measured and calculated results is 8.3% and the average relative error is about 5.7%. It can be seen that the peak optical power of LED system decreases from about 56.3 W measured 1 min after the initial operation to about 52.1 W measured 26 min after the initial operation. This is almost an 8.1% optical power reduction if the steady-state optical power value is used as a base value. The optical power decreases with time because the temperature of the heatsink increases gradually with time and consequently increases the junction temperature. An increase in junction temperature results in a reduction of luminous efficacy, causing the optical power to decrease.

The corresponding predicted CCT variation is plotted in Fig. 18. It can be seen that CCT of the passive LED system varies with time. The top and bottom region of CCT is 4042 and 3913 K, respectively. It is important to note that, the maximum CCT deviation of predicted results obtained with the PET theory is 129 K. The deviation in CCT is basically nonperceivable and meets the requirement set in the ANSI Standard C78.377 [23].

V. Conclusion

The integrating sphere with a photo-spectro-colorimeter system is primarily suitable for steady-state optical measurements and unsuitable for monitoring dynamic behavior of LED systems. In this paper, it is demonstrated that real-time measurements obtained from a photodetector system can be processed and used to develop and analyze PC-LED devices with the help of the dynamic PET theory. This method has been applied in an extended PC LED model to cover the optical power calculations of blue LED chip and phosphor layer independently. The proposed method involves a fast and simple measurement procedure based on the use of the photodetector and an oscilloscope. It has been used to model an LED power system with dynamic current ripple. The dynamic voltage output from the photodetector can be transformed into the dynamic optical power waveform in the time domain. The calculated and measured optical power results agree well even when they are obtained at different time frames after the LED system has been activated. Such good agreements confirm the feasibility and usefulness of using a photodetector system as a dynamic measurement tool for monitoring an LED system. The combined use of the photodetector and the dynamic PET theory provides a new tool for design engineers to perform optical, color, and thermal evaluations for optimal LED system designs.

References

[1] P. T. Chou, S. P. Ying, T. T. Chen, and C. K. Lee, "Study of different testing methods used in UV-LED optical measurement," *J. Display Technol.*, vol. 11, no. 12, pp. 1014–1017, Dec. 2015.

[2] H. T. Chen and S. Y. R. Hui, "Dynamic prediction of correlated color temperature and color rendering index of phosphor-coated white light-emitting diodes," *IEEE Trans. Ind. Electron.*, vol. 61, no. 2, pp. 784–797, Feb. 2014.

[3] S. Y. R. Hui and Y. X. Qin, "A general photo-electro-thermal theory for light-emitting-diode (LED) systems," *IEEE Trans. Power Electron.*, vol. 24, no. 8, pp. 1967–1976, Aug. 2009.

[4] S. Y. R. Hui, H. T. Chen, and X. H. Tao, "An extended photoelectrothermal theory for LED systems: A tutorial from device characteristic to system design for general lighting [invited paper]," *IEEE Trans. Power Electron.*, vol. 27, no. 1, pp. 4571–4583, Nov. 2012.

[5] H. Hayashi *et al.*, "Thermally engineered flip-chip InGaN/GaN well-ordered nanocolumn array LEDs," *IEEE Photon. Technol. Lett.*, vol. 27, no. 22, pp. 2343–2346, Nov. 2015.

[6] J. C. W. Lam and P. K. Jain, "A high power factor, electrolytic capacitorless AC-input LED driver topology with high frequency pulsating output current," *IEEE Trans. Power Electron.*, vol. 30, no. 2, pp. 943–955, Feb. 2015.
[7] G. G. Pereira, M. A. D. Costa, J. M. Alonso, M. F. D. Melo, and C. H. Barriquello, "LED driver based on input current shaper without electrolytic capacitor," *IEEE Trans. Ind. Electron.*, vol. 64, no. 6, pp. 4520–4529, Jan. 2017.
[8] D. G. Lamar, M. Arias, A. Fernandez, J. A. Villarejo, and J. Sebastian, "Active input current shaper without an electrolytic capacitor for retrofit lamps applications," *IEEE Trans. Power Electron.*, vol. 32, no. 5, pp. 3908–3919, May 2017.
[9] G. M. Soares, P. S. Almeida, J. M. Alonso, and H. A. C. Braga, "Capacitance minimization in offline LED drivers using an active ripple-compensation technique," *IEEE Trans. Power Electron.*, vol. 32, no. 4, pp. 3022–3033, Apr. 2017.
[10] S. Y. R. Hui, S. N. Li, W. Chen, X. H. Tao, and W. M. Ng, "A novel passive LED drivers with long lifetime," *IEEE Trans. Power Electron.*, vol. 25, no. 10, pp. 2665–2672, Oct. 2010.
[11] S. N. Li, S. C. Tan, C. K. Lee, E. Waffenschmidt, S. Y. R. Hui, and C. K. Tse, "A survey, classification, and critical review of light emitting diode drivers," *IEEE Trans. Power Electron.*, vol. 31, no. 2, pp. 1503–1516, Feb. 2016.
[12] D. Y. Kang, E. Wu, and D. M. Wang, "Modeling white light-emitting diodes with phosphor layers," *Appl. Phys. Lett.*, vol. 89, no. 23, Dec. 2006, Art. no. 231102.
[13] V. Y. F. Leung, A. Lagendijk, T. W. Tukker, A. P. Mosk, W. L. Ijzerman, and W. L. Vos, "Interplay between multiple scattering, emission, and absorption of light in the phosphor of a white light-emitting diode," *Opt. Express.*, vol. 22, no. 7, pp. 8190–8204, Apr. 2014.
[14] W. L. Vos, T. W. Tukker, A. P. Mosk, A. Lagendijk, and W. L. Ijzerman, "Broadband mean free path of diffuse light in polydisperse ensembles of scatterers for white light-emitting diode lighting," *Appl. Opt.*, vol. 52, no. 12, pp. 2602–2609, Apr. 2013.
[15] M. L. Merstska, R. Uppu, G. Vissenberg, A. Lagendijk, W. L. Ijzerman, and W. L. Vos, "Analytical modeling of light transport in scattering materials with strong absorption," *Opt. Express*, vol. 25, no. 20, pp. A906–A921, Oct. 2017.
[16] Datasheet: PDA36A-EC, "PDA36A-EC - Si switchable gain detector user guide," THORLABS, 2006. [Online]. Available: https://www.thorlabschina.cn/thorproduct.cfm?partnumber=PDA36A-EC
[17] Measurement of LEDs. CIE 127-2007, 2007. [Online]. Available: http://www.cie.co.at/publications/measurement-leds
[18] S. Y. R. Hui and W. Chen, "Apparatus and methods of operation of passive LED lighting equipment," U.S. Patent application 12/544,545 20 Aug. 2009.
[19] H. T. Chen, S.-C. Tan, and S. Y. R. Hui, "Color variation reduction of GaN-based white light- emitting diodes via peak-wavelength stabilization," *IEEE Trans. Power Electron.*, vol. 29, no. 7, pp. 3709–3719, Jul. 2014.
[20] X. H. Tao and S. Y. R. Hui, "Dynamic photoelectrothermal theory for LED systems," *IEEE Trans. Ind. Electron.*, vol. 59, no. 4, pp. 1751–1759, Apr. 2012.
[21] H. T. Chen, S. C. Tan, and S. Y. R. Hui, "Chromatic, photometric and thermal modeling of LED systems with non-identical LED devices," *IEEE Trans. Power Electron.*, vol. 29, no. 12, pp. 6636–6647, Dec. 2014.
[22] A. T. L. Lee, H. T. Chen, S. C. Tan, and S. Y. R. Hui, "Precise dimming and color control for LED systems," *IEEE Trans. Power Electron.*, vol. 31, no. 1, pp. 65–80, Jan. 2016.
[23] *Specifications for Chromaticity of Solid State Lighting Products*, American National Standard ANSI C78.377, 2008.

Huanting Chen received the Ph.D. degree in wireless physics from Xiamen University, Xiamen, China, in 2010.

He was a Senior Research Associate with the Department of Electronic Engineering, City University of Hong Kong, Hong Kong, in 2011. He was a Postdoctoral Fellow with the Department of Electrical and Electronic Engineering, The University of Hong Kong, Hong Kong, from 2012 to 2016. He is currently a Professor with the College of Physics and Information Engineering, Minnan Normal University, Zhangzhou, China. His research interests include solid-state lighting theory and technology.

Albert T. L. Lee (M'13) received the B.Sc. degree (Hons.) in electrical engineering from the University of Wisconsin- Madison, Madison, WI, USA, in 1994, the M.Sc. degree in electrical and computer engineering from the University of Michigan, Ann Arbor, MI, USA, in 1996, and the Ph.D. degree in electronic and computer engineering from the Hong Kong University of Science and Technology, Hong Kong, in 2014, respectively.

In 1996, he joined Intel Corporation, Hillsboro, OR, USA, as a Senior Component Design Engineer and was involved in the development of Intel's P6 family microprocessors. In 2001, he was a Senior Corporate Application Engineer with the System-Level Design Group, Synopsys, Inc., Mountain View, CA, USA. In 2003, he joined the Hong Kong Applied Science and Technology Research Institute Company, Ltd., and was an EDA Manager with the Wireline Communications Group. In 2006, he joined the Giant Electronics Limited as a Hardware Design Manager and became an Associate General Manager in 2008. He is currently a Research Associate with the Department of Electrical and Electronic Engineering, The University of Hong Kong, Hong Kong. He was named as one of the IEEE Transactions on Power Electronics' Outstanding Reviewers of 2016. His research interests include the areas of power electronics and control, LED lightings, emerging LED driver technologies, and wireless power transfer.

Siew-Chong Tan (M'06–SM'11) received the B.Eng. (Hons.) and M.Eng. degrees in electrical and computer engineering from the National University of Singapore, Singapore, in 2000 and 2002, respectively, and the Ph.D. degree in electronic and information engineering from the Hong Kong Polytechnic University, Hong Kong, in 2005.

He is currently a Professor with the Department of Electrical and Electronic Engineering, The University of Hong Kong, Hong Kong. He was a Visiting Scholar with Grainger Center for Electric Machinery and Electromechanics, University of Illinois at Urbana-Champaign, Champaign, from September to October 2009, and an Invited Academic Visitor of Huazhong University of Science and Technology, Wuhan, China, in December 2011. His research interests include the areas of power electronics and control, LED lightings, smart grids, and clean energy technologies. He is a Co-Author of the book *Sliding Mode Control of Switching Power Converters: Techniques and Implementation* (Boca Raton: CRC, 2011).

Prof. Tan is currently an Associate Editor for the IEEE Transactions on Power Electronics.

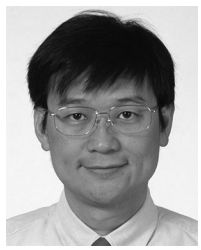

S. Y. (Ron) Hui (M'87–SM'94–F'03) received the B.Sc.Eng (Hons) degree in electrical and electronic engineering from the University of Birmingham, Birmingham, U.K., in 1984, and the D.I.C. and Ph.D. degrees in electrical engineering from the Imperial College London, London, U.K., in 1987.

He is currently the Philip Wong Wilson Wong Chair Professor with the University of Hong Kong, Hong Kong, and a Chair Professor with Imperial College London. He has authored or coauthored more than 260 refereed journal publications. More than 55 of his patents have been adopted by industry. His research interests include power electronics, wireless power, sustainable lighting, and smart grids. His inventions on wireless charging platform technology underpin key dimensions of Qi, the world's first wireless power standard, with freedom of positioning and localized charging features for wireless charging of consumer electronics. He also developed the Photo-Electro-Thermal Theory for LED Systems.

Prof. Hui was the recipient of the IEEE Rudolf Chope R&D Award from the IEEE Industrial Electronics Society and the IET Achievement Medal (The Crompton Medal) in 2010 and the IEEE William E. Newell Power Electronics Award in 2015. He is a Fellow of the Australian Academy of Technological Sciences & Engineering (since 2010), the US Academy of Inventors (since 2018), and the Royal Academy of Engineering, U.K. (since 2016).